Stability of martensite with pulsed electric current in dual-phase steels

Stability of martensite with pulsed electric current in dual-phase steels

W.J. Lu, R.S. Qin

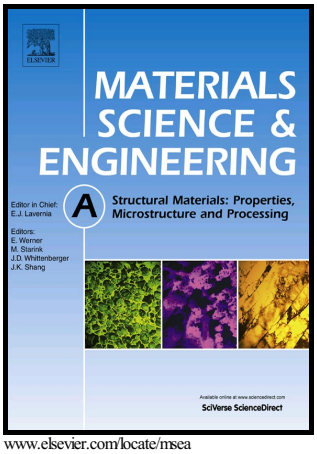

www.elsevier.com/locate/msea

PII: S0921-5093(16)31059-0
DOI: http://dx.doi.org/10.1016/j.msea.2016.08.123
Reference: MSA34081

To appear in: *Materials Science & Engineering A*

Received date: 27 August 2016
Revised date: 30 August 2016
Accepted date: 31 August 2016

Cite this article as: W.J. Lu and R.S. Qin, Stability of martensite with pulsed electric current in dual-phase steels, *Materials Science & Engineering A* http://dx.doi.org/10.1016/j.msea.2016.08.123

Stability of martensite with pulsed electric current in dual-phase steels

W.J. Lu[1*], R.S. Qin[2]

[1]Department of Materials, Imperial College London, Exhibition Road, London SW7 2AZ, United Kingdom

[2]Department of Engineering & Innovation, The Open University, Milton Keynes MK7 6AA, UK

[*]Corresponding authors. Tel.: +44 (0)20 7562 0419. *E-mail addresses:* w.lu@imperial.ac.uk (W.L. Lu).

Abstract

Softening frequently occurs in dual-phase steels under isothermal tempering of martensite. Recently, non-isothermal tempering is implemented to decrease the softening process in dual-phase steels. Here, we have discovered using high power electropulsing treatment can significantly enhance the strengthening effects via the formation of ultrafine-grained ferrite with nano-cementite particles in tempered martensitic-ferritic steels. To the best our knowledge, electropulsing treatment is a proper candidate to retard even to recovery the softening problems in the tempering of martensite in comparison with other isothermal and non-isothermal tempering methods.

Keywords:

dual-phase steel; tempering martensite; softening effect; nano-crystallization; electropulsing treatment

1. Introduction

Dual-phase, ferritic-martensitic steels with favourable combinations of high strength and good ductility have attracted significant attention recently in the automotive industries [1-5]. Although, dual-phase steels have outstanding mechanical properties compared with conventional steels, it has been reported that isothermal tempering of martensite (involving slow heating rate, long holding time and slow cooling rate) such as welding frequently leads to softening of the heated-affected zone (HAZ) i.e. a reduction in hardness for dual-phase steels [6-9].

In classical theory, the tempering of martensite occurs in four (temperature-related) stages during the softening process, as shown in Fig.1 [10]. It can be clearly seen that the hardness of martensitic steels, just as dual-phase steels, are significantly affected by temperature. When the temperature is heated up to 200 ^{o}C at stage 1, carbon atoms diffuse and segregate in some specific areas with a high-energy state, such as the grain boundaries. During stage 2, various carbides, such as ε-carbide, start to precipitate in the range, 200-400 ^{o}C. On further heating, cementite particles start to precipitate and spheroidize at grain boundaries at temperatures of 400-600 ^{o}C during stage 3. When the temperature exceeds 600 ^{o}C, most of the martensite laths have recrystallized and the cementite particles have coarsened during stage 4. The total hardness of a dual-phase steel decreases continuously with increasing temperature during the four stages of softening process. However, this softening (induced by the tempering of martensite) frequently causes premature failure in the HAZ of dual-phase steels during welding due to concentration of high strain in the softened regions [11-12]. Thus, many investigators have studied using non-isothermal tempering to replace isothermal tempering [6, 12-13]. Non-isothermal tempering, as carried out in e.g. Nd:YAG laser welding involves a high heating rate, a short holding time at the tempering temperature and a high cooling rate. It was found that the

non-isothermal tempering effectively decreases the softening by delaying stage 4 of the softening process [6]. Although, non-isothermal tempering is expected to decrease the hardness reduction, there is still a possibility of failure in the HAZ of dual-phase steel induced by softening. Thus, a way of overcoming the softening during the tempering of martensite in welding, is still urgently required to aid the application of dual-phase steels in many industrial installations.

One possible way of solving the above-mentioned difficulties is to use electropulsing treatment (EPT), which is an instantaneous, high- energy- input method. Previous studies using EPT on polycrystalline metals and alloys have shown that grain refinement can be achieved through the combination of thermal and electric effects generated in EPT [14-26]. Thus, the mechanical properties (associated with the changing of grain size) can be subsequently modified by EPT.

Most publications on dual-phase steels have concentrated on the methods to decrease the reduction of hardness (softening) during tempering of martensite [6, 8, 27]. Consequently, the present work has been focused, principally, on designing a novel method to retard (or overcome) the softening during the tempering of martensite in dual-phase steels. The strengthening mechanism is responsible for the microstructure evolution under EPT observed in rapidly tempered specimens due to the thermal and electric effects. Therefore, in this study, the cold-rolled, dual-phase steels have been treated with EPT. The tensile mechanical behaviour and the Vickers hardness were measured along with the microstructure evolution, which was monitored using SEM and TEM. These methods provide direct evidence of grain refinement and data for the kinetics and thermodynamics model. This indicates improvements in all mechanical properties of the dual-phase steel, which has not been reported previously for steels of this grade.

2. Materials and methods

The samples consisted of 1mm thick, dual-phase (DP600) steel plate containing ferrite and martensite phases (chemical composition (wt.%): 0.10C, 0.25Si, 1.70Mn, 0.02P, 0.005S, 0.040Al and balance Fe). The steel plate was cold rolled to the thickness of 0.5 mm through five passes and the total thickness reduction was 50 %. The steel samples were cut into dog-bone shape specimens (gauge length and width were 24.0 and 5.0 mm, respectively) with their longest edge perpendicular to the rolling direction, as shown in Fig. 2. In order to determine the effect of EPT, two sample groups were randomly selected and then one was subjected to EPT and the other used as a control (ie, without EPT). EPT was performed by converting the direct current into a pulsed electric current and the waveform of pulsed current was monitored, in-situ, by a digital storage oscilloscope, as shown in Fig. 2. The pulsed electric current was applied by using, cathode and anode clips to clamp to the steel sample. The pulsed electric current was applied for a total duration of 110 μs and had a peak current density 5.67×10^{9} Am^{-2} at ambient temperature. A thermocouple displayed in Fig. 2 was connected with sample specimen and the peak temperature was recorded immediately after EPT.

High-resolution scanning electron microscopy (SEM) and transmission electron microscopy (TEM) were to characterize the microstructure of treated samples and identify the phases present. The sample specimens were ground, polished and etched in 2 wt. % Nital for 5s for SEM analysis. The grain size and volume fraction of each phase were determined using, optical microscopy with ×100 magnification. This was used to randomly record the microstructure of samples at least 10 times and were then calculated by Image J. For TEM analysis, the specimens were mechanically polished to a thickness of 30 μm, punched to prepare disk specimens with a

diameter of 3 mm by a copper disk cutter, and then jet polished to prepare thin foil specimens using a mixture solution of perchloric acid (10 %) and acetic acid (90 %) with 20 V at 15 ^{o}C.

The mechanical properties of the samples, before and after EPT, were measured at room temperature using a Zwick/Roell tensile test machine, with a strain rate 10^{-3} s^{-1}. The Software test Xpert II was used to fit and derive the yield stress (0.2% proof stress) and the elongation. A micro compact, hardness test machine (Zwick 3103 IRHD) with 10 kg load was used to measure the hardness value of samples. The electrical resistance of the samples (with and without EPT) was measured using a micro-ohmmeter (DO5000 series) at room temperature.

3. Results

3.1 Effects of EPT on microstructure evolutions

The optical microstructure of the cold-rolled steel specimen and its XRD spectrum are shown in Figs 2c and 2d, respectively. It clearly shows the presence of only two phases. The martensite phase (black regions) is randomly distributed along the grain boundary of the ferrite matrix (grey regions). The volume fraction of ferrite and martensite were calculated to be 63.4 % and 36.6 %, respectively from Image J. It was found that, after applying EPT, the martensite laths were significantly altered without changing the portion of the two regions, as shown in SEM micrographs (Fig. 3).

Direct evidence of refinement can be clearly observed in martensitic regions (from micro-scale laths to nano-scale particles) in Fig. 3. TEM observations and selected area diffraction patterns (SADP) have been conducted in order to observe the microstructure of the samples (with and without EPT) and to detail and identify the nature of the nano-particles. The bright field images

of the morphologies of the martensite laths and the corresponding SADP, for the sample without EPT (Fig. 3e and g, respectively). After EPT, a high density of nano-particles with average size 48±8 nm were found around the grain boundary of the ferrite (indicated by arrows in Fig. 3f) and SADP confirmed that these nano-particles were cementite (Fig. 3h). These nano-sized cementite particles have an orientation relationship ($[012]_{\alpha}$ // $[101]_{\theta}$) with the ferrite matrix [6]. In addition, the original martensite laths (Fig. 3e) were partially decomposed into ultra-fine-grained ferrite with a size about 78±13 nm (Fig. 3f) after applying EPT.

3.2 Effects of EPT on mechanical properties

Standard stress-strain curves of samples (without and with EPT) were measured and are plotted in Fig. 4. It was found that EPT increased significantly both the yield stress and ultimate tensile strength of the steel sample whereas the elongation was only slightly affected by EPT (see Table. 1). The Vickers hardness of samples was increased from 301±8 HV to 364±12 HV after EPT. The above-mentioned results indicate that EPT has a positive effect in the quest to optimize the mechanical properties.

4. Discussion

4.1 Thermal effect of EPT

In general, the effects of EPT on microstructure evolution of polycrystalline metals and alloys can be divided into two types, namely the thermal and electric effects [28-33]. For the thermal effect of EPT, the temperature increase induced by joule heating can be expressed as

$\Delta T = j^2 \Delta t \rho / C_p d$ [28, 30-31], where j the current density (5.67×10^9 A/m^2), ρ is the electrical resistivity of the steel sample (9.64×10^{-7} Ωm), Δt is the pulse duration (110 μs), C_p is the specific heat of steel sample (450 J/kg K) and d is the density of steel sample (7.9×10^3 kg/m^3). The temperature increase resulting from EPT is calculated to be about 685 ^{o}C, which corresponds to stage 4 in the softening process, as can be seen in Fig. 5a. This calculated temperature (685 ^{o}C) is consistent with the peak temperature (672 ^{o}C) measured by a thermocouple after EPT.

A dramatic softening effect (reduction in hardness) occurs in dual-phase steel at stage 4 during the isothermal tempering of martensite, due to the coarsening of cementite and the decomposition of martensite (replaced by ferrite) [6, 10]. For example, The hardness of as-received, dual-phase steels decreased from (301±8 HV) to (190±3 HV) and (179±1 HV) with isothermal tempering at around 690 ^{o}C, for periods of (300s) and (5400s) , respectively [6], as shown in Fig .5b. Even if the non-isothermal tempering of martensite can be delayed to stage 4, the softening process still exists, which retards the reduction of hardness from 301±8 HV to 269±7 HV [7]. However, our experiment shows the softening process was inhibited by the tempering of martensite in dual-phase steels under EPT. The Vickers hardness of steel sample with EPT was 364±12 HV, which has an increase of 20.9 % over that of the steel sample without EPT (301 HV). Furthermore, standard stress-strain curves for samples, with and without EPT, are shown in Fig. 4. The yield stress for without EPT and with EPT, samples were recorded as from 773.26 MPa to 1074.66 MPa. This indicates that EPT strengthens the tempering of martensite during stage 4 of the softening process in dual-phase steels, which cannot be interpreted on the basis of the thermal effect of EPT alone.

4.2 Electric effect of EPT

Grain refinement is an effective method of improving the mechanical properties (such as Vickers hardness and yield stress, based on the Hall-Petch relationship) of polycrystalline metals and alloys. The relationship between stress and hardness is [26-28] is well known:

$$3\sigma_y = H_v \tag{4.1}$$

where σ_y is yield stress and H_v is the Vickers hardness. The yield stress and hardness can be expressed empirically as:

$$\sigma_y = \sigma_0 + k_y d^{-1/2} \tag{4.2}$$

$$H_y = H_0 + k_H d^{-1/2} \tag{4.3}$$

where σ_0 and H_0 are friction stress constants for tensile and hardness measurement, respectively, k_y and k_H are the unpinning parameters (breaking away of dislocation from interstitial sites) during tensile and hardness measurements, respectively; d is the grain size.

According to above-mentioned equations, the mechanical properties (i.e. yield stress and hardness) of dual-phase steels are strongly dependent to the grain size. This may be used to interpret the abnormal effect of EPT on the tempering of martensite in dual-phase steels. The microstructural characterization and its associated mechanical property data are in agreement with the yield stress and Vickers hardness data for the steel sample; these properties show significant improvement during the tempering of martensite under EPT which is associated with the formation of ultrafine-grained ferrite with nano-cementite particles. This strengthening

mechanism induced by EPT is completely different from the softening mechanisms of isothermal or non-isothermal tempering [6, 8, 12]. This improvement of mechanical properties associated with grain refinement can be analysed by two aspects of the electric effects of EPT: namely, kinetic and thermodynamic effects.

4.2.1 Kinetic effects of electric current

Cold working can effectively increase the dislocation density around the boundaries of martensite laths [34] in strain- free dual-phase steel samples, as shown in Fig. 6a. From the kinetic viewpoint, it is well known that EPT has a significant effect on the dislocation migration behaviour (i.e. intersection and annihilation of dislocations) in cold-formed materials [35]. This is due to the electron wind force generated by EPT, which can scatter unevenly around dislocations and which, subsequently, reduces the kinetics barrier between two neighbour dislocations [28, 30-32]. Therefore, the mobility of dislocations can be enhanced, which can be expressed as [36]:

$$J = \frac{2NeZ^{*}D\rho j_{m} f\tau_{p}}{kT} \tag{4.4}$$

where ρ is the electrical resistivity of steel sample, f is the frequency of EPT, j_m is the current density of EPT, τ_p is the duration of EPT, J is the additional atomic diffusion flux, N is the density of atoms, Z^* is effective valence of the Fe ion (+3), e is the charge on an electron, K is the Boltzmann constant and T is the absolute temperature. From Equ. 4.4, it can be clearly seen that the current density of EPT is proportional to the atomic diffusion flux. This proportional relationship indicate that EPT greatly increases the probability of intersection and annihilation of

the dislocation, as shown in Fig. 6b. In general, EPT can significantly reduce the dislocation density via annihilation of dislocation in heavily deformed metals and alloys [17-18, 37]. However, EPT also promotes the interaction of dislocation to form dislocation substructures (e.g. sub-grains) [40]. These sub-grains induced by dislocation have relatively high energy state, which can provide potential nucleation sites for secondary particles formation within matrix [41]. Thus, secondary particles, such as cementite, generally, nucleate at the intersection site of two partial dislocations at high temperature. EPT can promote a large number of nano-cementite particles within tempered martensite regions, as can be seen in Fig. 6c.

4.2.2 Thermodynamic of electric current

Since the temperature induced by EPT is about 685 ^{o}C, most martensite laths decomposed instantaneously to cementite and ferrite at this temperature range [6, 8 12]. From the thermodynamic point of view, the Gibbs free energy associated with the recrystallization process, especially the nucleation rate of ferrite can be influenced by EPT [14-26]. According to classical nucleation theory, when EPT is applied, the nucleation rate for ferrite, can be expressed as [18, 24, 37-38]:

$$I_e = I_r \exp(\frac{-\Delta G_{elec}}{RT}) \tag{4.5}$$

where I_r is the nucleation rate of the cold-rolled steel sample without EPT, R is the Boltzmann constant, T is the absolute temperature, ΔG_{elec} is the additional Gibbs free energy induced by EPT. The ΔG_{elec} can be, generally, defined as [39]:

$$\Delta G_{elec} \propto j^2 \Delta v K \frac{(\alpha_B - \alpha_A)}{(\alpha_B + 2\alpha_A)} \tag{4.6}$$

where j is the current density, ΔV is the volume of austenite particle, K is a material constant (K), α_B and α_A are the electrical conductivity of cementite and ferrite, respectively. It is well known that the electrical conductivity of the ferrite phase is higher than that of cementite in steels ($\sigma_\theta < \sigma_\alpha$). It can be predicted that $\Delta G_{elec} \leq 0$. Thus the more negative the value of ΔG_{elec} the greater (i.e. more positive) the value of nucleation rate (I_e). Simultaneously, dislocations, as one of the common defects, have a negative effect on the electrical conductivity of a steel sample [28, 32]. Since the EPT enhances the probability of annihilation of dislocations; this will result in higher electrical conductivity of the steel sample due to the fewer dislocations after EPT. Our measurements indicate that the electrical conductivity for the steel samples, without and with, EPT are 1.04×10^6 Ω·m and 1.47×10^6 Ω·m, respectively. The electrical conductivity of the specimen is increased by 41.4 % with EPT. Thus, EPT can enhance the nucleation rate of ferrite and effectively retard the growth rate of ferrite during recrystallization. Eventually, ultrafine-grained ferrite matrix within tempered martensite regions are produced by using EPT. In addition, the phase transformation (decomposition of martensite to ferrite and cementite) associated with Gibbs free energy change can also be affected by EPT at a temperature about 685 ^oC due to different electrical conductivities [28-32, 42]. It is well known that the Gibbs free energy of whole system (steel) contains four typical components: chemical free energy, interface energy (grain boundary and phase boundary), strain-induced energy and current free energy when an electrical current going through the steel specimen [42]. Due to different electrical conductivity of phases existed in steel, the current free energy can be changed subsequently by EPT. This change of current free energy can cause the different change of phase transformation [30]. Thus, it has been observed that electric current delay the softening process in the stage 4, which implies

that the decomposition of martensite was delayed by EPT due to higher electrical conductivity of marteniste.

4.2.3 EPT on mechanical properties

All mechanical properties of dual-phase steels (namely yield stress, ultimate tensile stress and hardness) were all significantly increased EPT without losing elongation; this was mainly attributed to the formation of ultrafine-grained ferrite with nano-cementite particles. From the kinetic and thermodynamic aspects of EPT, the microstructure evolution can be due to various mechanisms (such as dislocation- migration and electrical conductivity changes, associated with nucleation rate during recrystallization). These experimental results and theoretical analysis, indicate that EPT is a potential candidate to retard (or even to recover) the softening problems encountered in the tempering of martensite in comparison during isothermal and non-isothermal tempering.

5. Conclusions

Electropulse-tempering can effectively strengthen the tempering of martensite by forming ultrafine-grained ferrite with nano-cementite particles. This is mainly attributed to the accelerated dislocation migration (kinetic) and to the enhanced nucleation rate of ferrite during recrystallization (thermodynamic) by EPT. Therefore, it is possible to use such phenomena to recover the softening which occurs in tempering of martensite in dual-phase steels; thus, the thermal and electric effects of EPT are more effective than isothermal or non-isothermal tempering in dealing with softening.

Acknowledgements

The work was financially supported by EPSRC (No. EP/J011460/1), TATA Steel and the Royal Academy of Engineering at United Kingdom. The authors are grateful to Professor Kenneth C. Mills at Imperial College London for fruitful discussions.

References

[1] C.W. Zheng, D. Raabe, D.Z. Li, Prediction of post-dynamic austenite-to-ferrite transformation and reverse transformation in a low-carbon steel by cellular automaton modeling, Acta Mater. 60 (2012) 4768-4779.

[2] M. Calcagnotto, D. Ponge, D. Raabe, Effect of grain refinement to 1 μm on strength and toughness of dual-phase steels, Mater. Sci. Eng. A. 527 (2010) 7832-7840.

[3] M. Delincé, Y. Bréchet, J.D. Embury, M.D. Geers, P. J. Jacques, T. Pardoen, Structure-property optimization of ultrafine-grained dual-phase steels using a microstructure-based strain hardening model, Acta Mater. 55 (2007) 2337-2350.

[4] K. Mukherjee, S.S. Hazra, M. Militzer, Grain refinement in dual-phase steels, Metall. Mater. Trans. A 40 (2009) 2145–2159.

[5] G. Avramovic-Cingara, Y. Ososkov, M.K. Jain, D.S. Wilkinson, Effect of martensite distribution on damage behaviour in DP600 dual phase steels, Mater. Sci. Eng. A, 516 (2009) 7–16.

[6] V.H. Baltazar Hernandez, S.S. Nayak, Y.Zhou, Tempering of martensite in dual-phase steels and its effects on softening behavior, Metall. Mater. Trans. A 42 (2011) 3115–3129.

[7] N. Sreenivasan, M. Xia, S. Lawson, Y. Zhou, Effect of Laser Welding on Formability of DP980 steel, J. Eng. Mater. Technol. 130 (2008) 041004.

[8] D.C. Saha, D. Westerbaan, S.S. Nayak, E. Biro, A.P. Gerlich, Y. Zhou, Microstructure-properties correlation in fiber laser welding of dual-phase and HSLA steels, Mater. Sci. Eng. A, 607 (2014) 445–453.

[9] E. Biro, J.R. McDermid, S. Vignier, Y. Norman Zhou, Decoupling of the softening processes during rapid tempering of a martensitic steel, Mater. Sci. Eng. A, 615 (2014) 395–404.

[10] H.K.D.H. Bhadeshia, R.W.K. Honeycombe, Steels: Microstructure and properties, 3rd editio. Elsevier Ltd., Butterworth-Heinemann, Oxford, UK, 2006.

[11] S.K. Panda, N. Sreenivasan, M.L. Kuntz, Y. Zhou, Numerical Simulations Experimental Results of Tensile Test Behavior of Laser Butt Welded DP980 Steels, Jounral Eng. Mater. Technol. 130 (2008) 769–776.

[12] M.S. Xia, E. Biro, Z.L. Tian, Y.N. Zhou, Effects of Heat Input and Martensite on HAZ Softening in Laser Welding of Dual Phase Steels, ISIJ Int. 48 (2008) 809–814.

[13] T. Furuhara, K. Kobayashi, T. Maki, Control of Cementite Precipitation in Lath Martensite by Rapid Heating and Tempering, ISIJ Int. 44 (2004) 1937–1944.

[14] T.P. Barnak, A.F. Sprecher, H. Conrad, Colony (grain) size reduction in eutectic Pb-Sn casting by electropulsing, Scr. Metall. 32 (1995) 879–884.

[15] Y.S. Chao, Z. H. Lai, K.Y. He, H.R. Er, Microstructural relaxation of amorphous alloy Fe79Si7B14 during electropulsing, Mater. Sci. Eng. A 181–182 (1994) 982–985.

[16] M. Gao, G.H. He, F. Yang, J.D. Guo, Z.X. Yuan, B.L. Zhou, Effect of electric current pulse on tensile strength and elongation of casting ZA27 alloy, Mater. Sci. Eng. A 337 (2002) 110–114.

[17] Y.B. Jiang, L. Guan, G.Y. Tang, C.H. Shek, Z.H. Zhang, Influence of electropulsing treatment on microstructure and mechanical properties of cold-rolled Mg-9Al-1Zn alloy strip, Mater. Sci. Eng. A 528 (2011) 5627–5635.

[18] Y.B. Jiang, L. Guan, G.Y. Tang, Z.H. Zhang, Improved mechanical properties of Mg–9Al–1Zn alloy by the combination of aging, cold-rolling and electropulsing treatment, J. Alloys Compd. 626 (2015) 297–303.

[19] J. Li, J.H. Ma, Y.L. Gao, Q.J. Zhai, Research on solidification structure refinement of pure aluminum by electric current pulse with parallel electrodes, Mater. Sci. Eng. A 490 (2008) 452–456.

[20] Z.H. Lai, H. Conrad, G.Q. Teng, Y.S. Chao, Nanocrystallization of amorphous Fe–Si–B alloys using high current density electropulsing, Mater. Sci. Eng. A 287 (2008) 238–247.

[21] D. Räbiger, Y.H. Zhang, V. Galindo, S. Franke, B. Willers, S. Eckert, The relevance of melt convection to grain refinement in Al-Si alloys solidified under the impact of electric currents, Acta Mater. 79 (2014) 327–338.

[22] A. Rahnama, R.S. Qin, Electropulse-induced microstructural evolution in a ferritic–pearlitic 0.14% C steel, Scr. Mater. 96 (2015) 17–20.

[23] Z.H. Xu, G.Y. Tang, S.Q. Tian, J.C. He, Research on the engineering application of multiple pulses treatment for recrystallization of fine copper wire, Mater. Sci. Eng. A 424 (2006) 300–306.

[24] X.F. Xu, Y.G. Zhao, B.D. Ma, J.T. Zhang, M. Zhang, Rapid grain refinement of 2024 Al alloy through recrystallization induced by electropulsing, Mater. Sci. Eng. A 612 (2014) 223–226.

[25] Q. Xu, G.Y. Tang, Y.B. Jiang, G.L. Hu, Y.H. Zhu, Accumulation and annihilation effects of electropulsing on dynamic recrystallization in magnesium alloy, Mater. Sci. Eng. A 528 (2011) 3249–3252.

[26] Q. Xu, G.Y. Tang, Y.B. Jiang, Thermal and electromigration effects of electropulsing on dynamic recrystallization in Mg-3Al-1Zn alloy, Mater. Sci. Eng. A 528 (2011) 4431–4436.

[27] N. Farabi, D.L. Chen, J. Li, Y. Zhou, S.J. Dong, Microstructure and mechanical properties of laser welded DP600 steel joints, Mater. Sci. Eng. A 527 (2010) 1215–1222.

[28] R.S. Qin, E.I. Samuel, A. Bhowmik, Electropulse-induced cementite nanoparticle formation in deformed pearlitic steels, J. Mater. Sci. 46 (2011) 2838–2842.

[29] W.J. Lu, R.S. Qin, Effects of Electropulsing on the Microstructure Evolution of 316L Stainless Steel, Adv. Mater. Res. 922 (2014) 441–445.

[30] W.J. Lu, X.F. Zhang, R.S. Qin, Electropulsing-induced strengthening of steel at high temperature, Philos. Mag. Lett. 94 (2014) 688–695.

[31] W.J. Lu, X.F. Zhang, R.S. Qin, Stability of precipitates under electropulsing in 316L stainless steel, Mater. Sci. Technol. 31 (2015) 1530-1535.

[32] R.S. Qin, A. Rahnama, W.J. Lu, X.F. Zhang, B. Elliott-Bowman, Electropulsed steels, Mater. Sci. Technol. 30 (2014) 1040–1044.

[33] X.F. Zhang, R. S. Qin, Electric current-driven migration of electrically neutral particles in liquids, 104 (2014) 114106-1-5.

[34] A. Inoue, K. Hashimoto, Amorphous and Nano-crystalline Materials: Preparation, Properties, and Application, 1st editio. Springer International Publishing Switerland, 2001.

[35] H. Conrad, Effects of electric current on solid state phase transformations in metals, Mater. Sci. Eng. A 287 (2000) 227–237.

[36] Y.B. Jiang, G.Y. Tang, L. Guan, S.N. Wang, Z.H. Xu, C.H. Shek, Y.H. Zhu, Effect of electropulsing treatment on solid solution behavior of an aged Mg alloy AZ61 strip, J. Mater. Res. 23 (2008) 2685–2691.

[37] Y. Liu, J.F. Fan, H. Zhang, W. Jin, H.B. Dong, B.S. Xu, Recrystallization and microstructure evolution of the rolled Mg – 3Al – 1Zn alloy strips under electropulsing treatment, J. Alloys Compd. 622 (2015) 229–235.

[38] Y.S. Zheng, G.Y. Tang, J. Kuang, X.P. Zheng, Effect of electropulse on solid solution treatment of 6061 aluminum alloy, J. Alloys Compd. 615 (2014) 849–853.

[39] Y. Dolinsky and T. Elperin, Thermodynamics of nucleation in current-carrying conductors, Phys. Rev. B 50 (1994) 52–58.

[40] X.X. Ye, X.P. Li, G.L. Song, G.Y. Tang, Effect of recovering damage and imrpoving microstcuture in the titanium alloy strip under high-energy electropulses, J. Alloys Compd. 616 (2014) 173-183.

[41] A. Weidner, R. Kolmorgen, I. Kubena, D. Kulawinski, T. Kruml, H. Biermann, Decomposition and preciitation process during thermo-mechnical fatigue of duples stainless steel, Metall. Mater. Trans. A 47A (2016) 2112-2124.

[42] W.J. Lu, R.S. Qin, Influence of κ-carbide interface structure on the formability of lightweight steels, Mater Des 104 (2016) 211-216.

Table

Table. 1: Mechanical properties (i.e. yield stress, UTS and elongation) of the steel samples (without and with EPT).

	Without EPT	With EPT	Increase by %
Yield stress (MPa)	773.26	1074.66	+38.98
UTS (MPa)	1034.25	1126.33	+8.90
Elongation (%)	3.31	3.12	-5.74

Fig. 1 Four stages in the softening process for the tempering of martenite in dual-phase steels.

Fig. 2 Schematic diagrams showing (a) experimental set-up of EPT; (b) a dog-bone shape sample (length: 24 mm; width: 5 mm and thickness: 0.5 mm); (c) an optical microstructure of dual-phase steel consisting of ferrite and martensite and (d) a XRD spectrum showing only body centred cubic phases (ferrite or martensite) exist in the steel sample. Note: F is ferrite and M is martensite.

Fig .3 SEM images of steel samples (a and c) without EPT at different magnifications, (b and d) with EPT at different magnifications; TEM bright images of steel samples (e) without EPT and (f) with EPT; selected area diffraction pattern (SADP) for (g) martensite laths and (h) ferrite grains with cementite particle. Note: α' is martensite, Tα' (α+θ) is tempering martensite and α is ferrite.

Fig. 4 Diagram showing typical tensile engineering stress-strain curves of dual-phase steel samples (with and without EPT).

Fig. 5 Diagrams showing a typical softening process contains four stages for the hardness of Fe-C martensitic steel tempered 1h at 100-700 ^{o}C and (b) the hardness of dual-phase steels tempered at about 700 ^{o}C for 110 μs (EPT), 0.1s<t<1 s (non-isothermal tempering), 300s (isothermal tempering) and 5400s (isothermal tempering), respectively [242].

Fig. 6 Diagrams showing (a) the microstructural evolution of dislocations in cold-formed steel sample, (b) the effect of EPT on intersection and annihilation of two partial dislocations and (c) the formation of ultrafine-grained ferrite with nano-cementite particles after EPT.

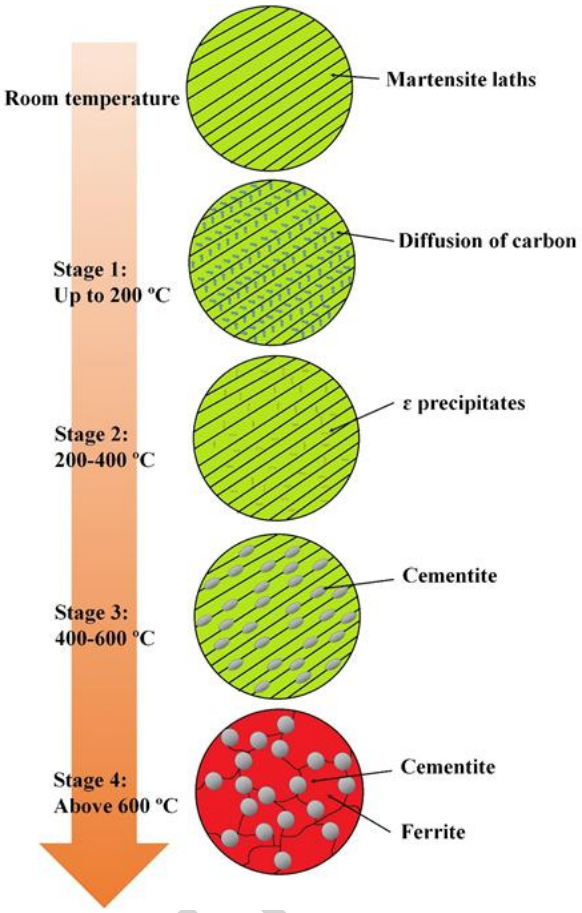
Room temperature
Martensite laths
Stage 1:
Up to 200 °C
Diffusion of carbon
Stage 2:
200-400 °C
ε precipitates
Stage 3:
400-600 °C
Cementite
Stage 4:
Above 600 °C
Cementite
Ferrite

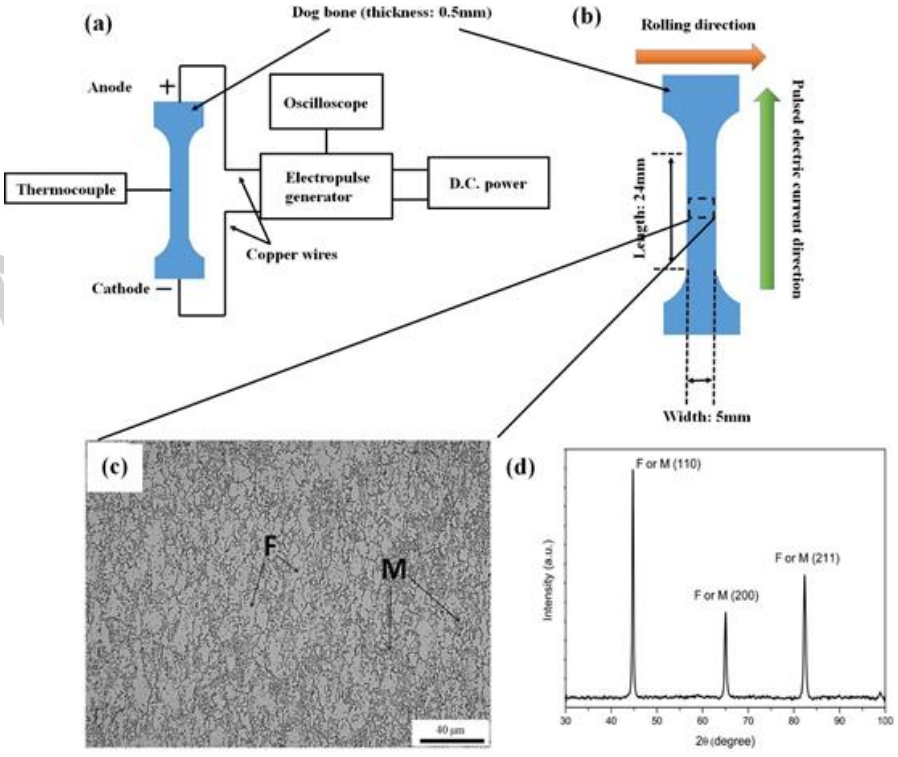
(a)
Dog bone (thickness: 0.5mm)
Anode
+
Oscilloscope
Thermocouple
Electropulse generator
D.C. power
Copper wires
Cathode
−
(b)
Rolling direction
Pulsed electric current direction
Length: 24mm
Width: 5mm
(c)
F
M
40 μm
(d)
F or M (110)
F or M (200)
F or M (211)
Intensity (a.u.)
30
40
50
60
70
80
90
100
2θ (degree)

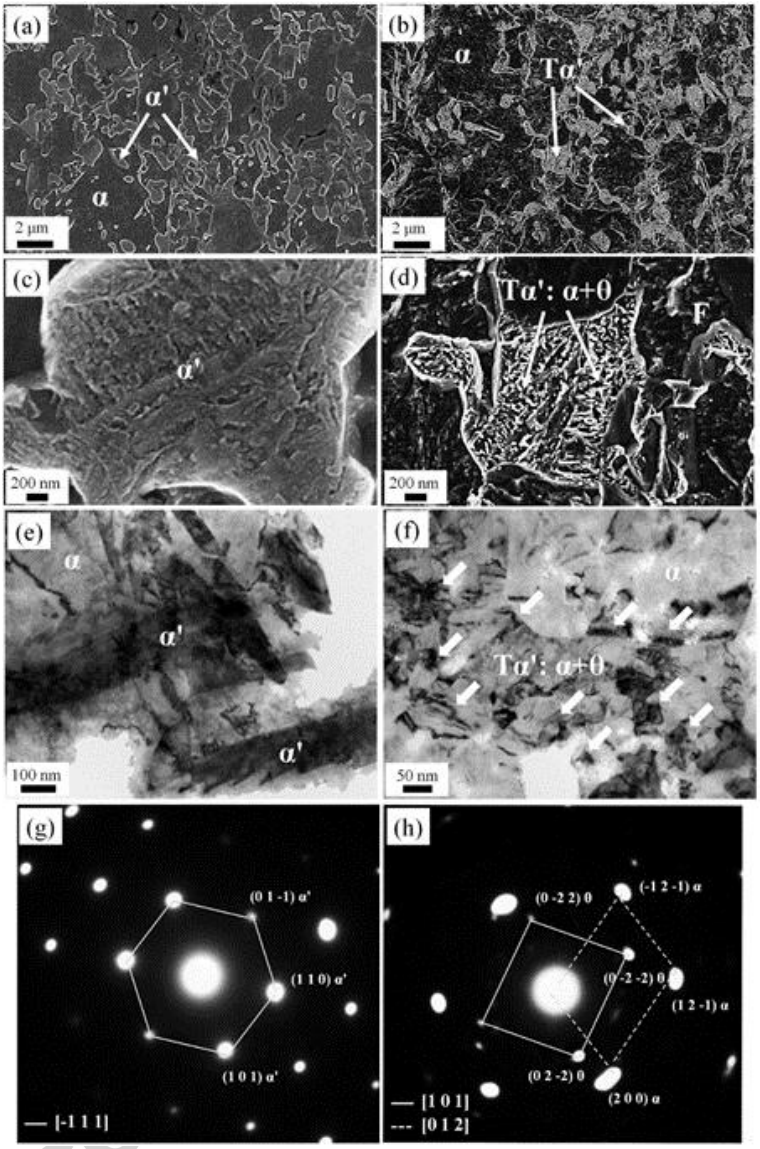

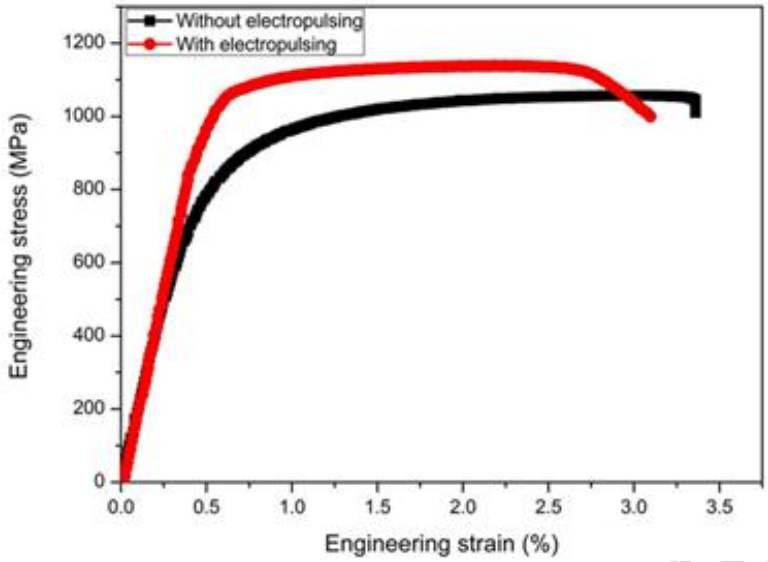
Without electropulsing
With electropulsing
Engineering stress (MPa)
Engineering strain (%)
0
200
400
600
800
1000
1200
0.0
0.5
1.0
1.5
2.0
2.5
3.0
3.5

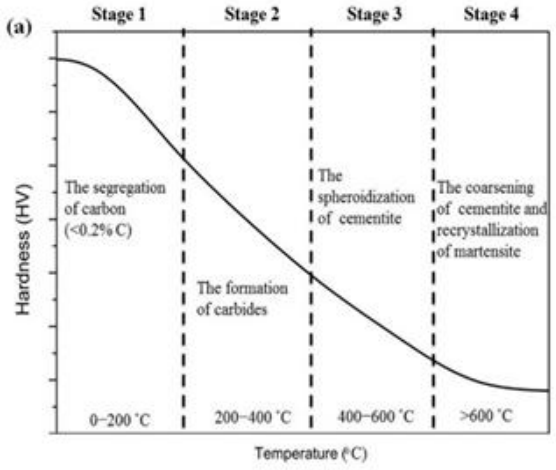
(a)
Stage 1
Stage 2
Stage 3
Stage 4
Hardness (HV)
The segregation of carbon (<0.2% C)
The formation of carbides
The spheroidization of cementite
The coarsening of cementite and recrystallization of martensite
0–200 °C
200–400 °C
400–600 °C
>600 °C
Temperature (°C)

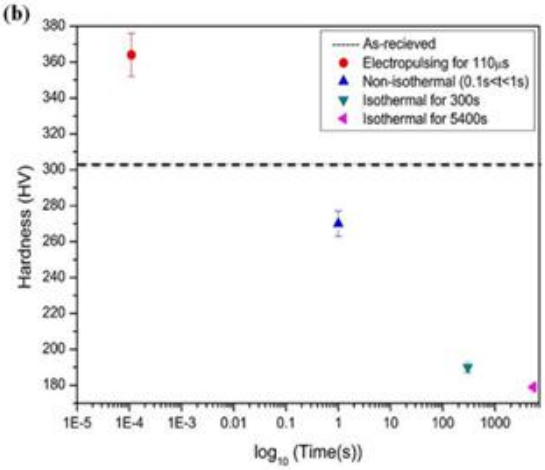
(b)
As-recieved
Electropulsing for 110μs
Non-isothermal (0.1s<t<1s)
Isothermal for 300s
Isothermal for 5400s
Hardness (HV)
log10 (Time(s))
180
200
220
240
260
280
300
320
340
360
380
1E-5
1E-4
1E-3
0.01
0.1
1
10
100
1000